Component-wise damage detection by neural networks and refined FEs training

Journal of Sound and Vibration 509 (2021) 116255

Contents lists available at ScienceDirect

Journal of Sound and Vibration

journal homepage: www.elsevier.com/locate/jsvi

# Component-wise damage detection by neural networks and refined FEs training

A. Pagani *, M. Enea, E. Carrera

*Mul*$^2$ *Group, Department of Mechanical and Aerospace Engineering, Politecnico di Torino, Corso Duca degli Abruzzi 24, 10129 Torino, Italy*

ARTICLE INFO

Handling Editor: I. Trendafilova

*Keywords:*
Damage detection
Neural Networks
Higher-order finite elements
Carrera Unified Formulation

ABSTRACT

Multilayer perceptrons are utilized in this work for vibration-based damage detection of multi-component aerospace structures. A back-propagation algorithm is utilized along with Monte Carlo simulations and advanced structural theories for training Artificial Neural Networks (ANN's), which are able to detect and classify local damages in structures given the natural frequencies and the associated vibrations modes. The latter ones are feed into the network in terms of Modal Assurance Criterion (MAC), which is a scalar representing the degree of consistency between undamaged and damaged modal vectors. Dataset and ANN training process is carried out by means of Carrera Unified Formulation (CUF), according to which refined finite elements with component-wise capabilities can be implemented in a hierarchical and unified manner. The proposed results demonstrate that CUF-trained ANNs can approximate complete mapping of the damage distribution, even in case of low damage intensities and local defects in localized components (stringers, spar caps, webs, etc.).

## 1. Introduction

Structural health monitoring is becoming more and more critical in aircraft industries. Non-destructive tests (NDT), such as visual inspection, magnetic field tests, and ultrasounds, are usually performed as part of the aircraft maintenance program. Nevertheless, NTD tests have some limitations, above all the necessity to know in advance the location of the damage to be investigated. For this reason, research activities are focusing on developing damage detection methods capable of overcoming this limitation.

One of these methods involves the use of guided waves. The scattering of these waves gives information about the quantification and localization of the damage. A review of the different applications of guided waves for structural health monitoring is presented in [1]. Fibre Bragg grating (FBG) sensor [2] and intelligent coating monitoring [3] are also used for on-line structural health monitoring, in particular for aeronautical structures.

The proposed research investigates the effects of localized damages on the variation of the structure's vibrational characteristics (i.e. a change in natural frequencies or mode shapes). Two types of problems could be posed: the direct problem and the inverse problem.

The direct problem aims at determining the change in a given structure's dynamic parameters when damage location and severity are known. In [4], Hirwani and Panda investigated the influence of delamination in curved composite structures under pulse load. In [5], the authors proposed a new method for computing natural frequencies in a beam with multiple cracks, where the latter are represented through a rotational spring model. In [6], Capozucca performed a free vibration analysis on a cantilever CFRP beam that was damaged by introducing two notches ad the fixed end. Yang et al. [7] developed an algorithm for investigating the influence

* Corresponding author.
*E-mail addresses:* alfonso.pagani@polito.it (A. Pagani), marco.enea@polito.it (M. Enea), erasmo.carrera@polito.it (E. Carrera).

https://doi.org/10.1016/j.jsv.2021.116255
Received 19 March 2021; Received in revised form 14 May 2021; Accepted 28 May 2021
Available online 7 June 2021

of crack parameters on the frequencies and mode shapes of a cantilever beam under non-symmetric boundary conditions. Carrera et al. in [8] proposed a component-wise approach for free-vibration analysis of damaged aircraft structures. This formulation was also employed to analyse tapered composite [9] and civil structures [10].

In the inverse problem the damage location and the intensity in a structure are unknown, whereas the dynamic parameters such as natural frequencies and mode shapes (or a combination of thereof), Frequency Response Functions (FRF) and modal strain energy are given. Kosmatka and Ricles [11] used dynamic parameters to perform a sensitivity analysis to estimate mass or stiffness variation in a structure. Fayyad et al. [12] proposed the Combined Parameters Index (CPI), which compared the reduction in stiffness with the decrease in the natural frequencies and with the change in mode shape. In [13], the authors solved an optimization problem for damage detection purpose by using natural frequencies as input. In [14], Ruotolo solved another optimization problem, but in this case, both natural frequencies and mode shapes were considered.

Recently, the general improvement of the computational performances pushed the research towards a machine learning approach for damage detection purpose, which facilitated the solving of this problem and allowed to investigate more complex structure (in terms of geometry and/or number of cracks). In this work, Artificial Neural Network (ANN) method has been used. Some studies are presented hereafter.

Sahin and Shenoi proposed a combination of global (shift in natural frequencies) and local (curvature mode shapes) dynamic analysis data as input for the ANN. This method has been tested on beam-like structures [15] and laminated composites [16]. In [17], Das and Pahri used the relative deviation of the first three natural frequencies and mode shapes of a cantilever beam to train the ANN. They compared the numerical results with experimental values. Suresh et al. [18] proposed a modular approach for identifying crack location and depth in a beam. Two different neural networks have been trained, one for estimating the crack location and the second for crack depth. Jayasehar and Sumangala [19] investigated prestressed concrete beams. Natural frequency measurements were considered as dynamic data. Other parameters employed as input were deflection, crack width, first crack load, and ultimate load. Saeed et al. [20] computed natural frequencies and FRFs in damaged and undamaged curvilinear beams via FE analysis. The shift in these parameters (from undamaged to damaged) was then used to train four different types of ANNs. A comparison with another machine learning method (multiple adaptive neuro-fuzzy inference system, ANFIS) is also shown. Aydin and Kisi [21] introduced material and geometrical features of the beam in the neural network and, for the first time, used (besides natural frequencies) mode shape rotation deviations. In [22], Fathnejat et al. detect damage location with the Modal Strain Energy Based Index (MSEBI) as input for a Cascade Feed Forward Neural Network (CFFNN). The error between actual MSEBIs and the value guessed by the ANN is minimized through the Particle Swarm Optimization (PSO).

In this work, ANN have been used in combination with refined 1D models obtained through the Carrera Unified Formulation (CUF). According to the CUF theory, the displacement field in the cross-section is modelled via expansion functions, whose order is a parameter of the analysis [23,24].

One of the last development of the CUF formulation is the Component-Wise (CW) approach. It allows to separately model each component of the structure through the 1-D CUF Lagrange polynomial formulation for the cross-section displacement field. In [8] this approach has shown to be suitable for solving the direct problem through free-vibration analysis, thanks to the excellent accuracy and the low computational cost. The ANN has been used in this work, instead, to solve the inverse problem; i.e. to detect damage location and intensity, giving as input some dynamic parameters of the structure. These parameters are the natural frequencies of the first important modes and the Modal Assurance Criterion (MAC) matrix [25]. The MAC is a scalars parameter originally employed to characterize mode-to-mode variation between experiments and mathematical models. In this case, however, MAC is used to quantify the difference in the modes between damaged and undamaged structures.

The main advantage of the proposed CW approach is that it allows to introduce diverse damages independently in each component of the structure, thus leading to a component-oriented localization of the damage. Hence, a database formed by N samples is created through Monte Carlo simulations. Each sample is a structure with a different damage distribution. The database is used for the ANN training process, which will make the network able to predict unseen output.

The present paper is organized as follows: first, one-dimensional CUF models are introduced, then CW and damage modelling is discussed; subsequently, the characteristics of the ANN are presented. Then, the numerical results for a three-stringer spar and a complete NACA wing are discussed. Finally, the main conclusions are drawn.

## 2. Refined 1D models for free vibration analysis

In the case of slender, solid-section, homogeneous structures subject to bending phenomena, classical beam models (e.g., EBBM and TBM) provide a reasonably good approximation of the problem. On the other hand, it is evident that for damage detection and accurate free vibration analysis of damaged structures, theories able to deal with local phenomena and 3D strain effects are needed. Refined beam models can fulfil this requirement and, if sufficiently enriched kinematics is adopted, they can provide the same accuracy of 3D elasticity solutions with very low computational costs. In this paper, the Carrera Unified Formulation (CUF) is employed to automatically develop 1D refined models with an arbitrary number of terms in the kinematic field. The basic ideas and the main advantages of CUF are described in this section.

### 2.1. Carrera unified formulation

Consider a generic beam structure aligned along the y axis, which has boundaries $0 \leq y \leq L$. The cross-section $\Omega$ is normal to the beam axis $y$. The validity of the formulation is not affected by the shape of the cross-section. In the framework of the CUF, the kinematics of a beam model can be summarized as follows:

$$\mathbf{u}(x, y, z) = F_\tau(x, z)\mathbf{u}_\tau(y), \qquad \tau = 1, 2, \ldots, M \tag{1}$$

where $\mathbf{u}(x, y, z) = \{u_x(x, y, z) \quad u_y(x, y, z) \quad u_z(x, y, z)\}^T$ is the displacement vector; $F_\tau$ indicates the functions of the cross-section coordinates $x$ and $z$; $\mathbf{u}_\tau$ is the generalized displacement vector; $M$ indicates the number of terms in the expansion. The repeated subscript $\tau$ indicates summation, according to the Einstein notation. Moreover, the choice of $F_\tau$ and $M$ is arbitrary. Thus, the basis functions adopted to model the displacement field across the section can be different and expanded to any order.

The models known in the literature as LE (Lagrange expansion) are obtained considering Lagrange-like polynomials as cross-section expanding functions $F_\tau$, and they have only pure displacement variables.

In [26], several Lagrange polynomials have been employed in order to develop advanced beam theories, such as three-point linear (L3), four-point bi-linear (L4), and nine-point bi-quadratic (L9) polynomials. The isoparametric formulation was exploited to deal with arbitrary-shaped geometries. The Lagrange polynomials can be found in [27]. However, the interpolation functions for the L9 element are given here as an example

$$\begin{aligned} F_\tau &= \tfrac{1}{4}(\mathsf{r}^2 + \mathsf{r}\,\mathsf{r}_\tau)(\mathsf{s}^2 + \mathsf{s}\,\mathsf{s}_\tau) \qquad \tau = 1, 3, 5, 7 \\ F_\tau &= \tfrac{1}{2}\mathsf{s}_\tau^2(\mathsf{s}^2 - \mathsf{s}\,\mathsf{s}_\tau)(1 - \mathsf{r}^2) + \tfrac{1}{2}\mathsf{r}_\tau^2(\mathsf{r}^2 - \mathsf{r}\,\mathsf{r}_\tau)(1 - \mathsf{s}^2) \qquad \tau = 2, 4, 6, 8 \\ F_\tau &= (1 - \mathsf{r}^2)(1 - \mathsf{s}^2) \qquad \tau = 9 \end{aligned} \tag{2}$$

where $\mathsf{r}$ and $\mathsf{s}$ vary from $-1$ to $+1$, whereas $\mathsf{r}_\tau$ and $\mathsf{s}_\tau$ are the nine points' coordinates. The displacement field of an L9 beam theory will be:

$$\begin{aligned} u_x &= F_1\, u_{x_1} + F_2\, u_{x_2} + \cdots + F_9\, u_{x_9} \\ u_y &= F_1\, u_{y_1} + F_2\, u_{y_2} + \cdots + F_9\, u_{y_9} \\ u_z &= F_1\, u_{z_1} + F_2\, u_{z_2} + \cdots + F_9\, u_{z_9} \end{aligned} \tag{3}$$

where $u_{x_1}, \ldots, u_{z_9}$ are the displacement variables of the problem and they represent the translational displacement components of each of the nine centres of the L9 polynomial. If further refinements are needed, the cross-section can be discretized by using several L-elements. This is one of the essential characteristics of the CW approach, which is described in Section 3.

### 2.2. Finite element approximation

The FE approach is adopted to discretize the beam structure along the $y$-axis. This process is realized via a classical finite element technique, where the displacement vector is given by

$$\mathbf{u}(x, y, z) = F_\tau(x, z)N_i(y)\mathbf{q}_{\tau i}, \qquad \tau = 1, \ldots, M, \; i = 1, \ldots, p + 1 \tag{4}$$

$N_i$ stands for the shape functions of order $p$ and $\mathbf{q}_{\tau i}$ is the nodal displacement vector,

$$\mathbf{q}_{\tau i} = \left\{ q_{u_{x_{\tau i}}} \quad q_{u_{y_{\tau i}}} \quad q_{u_{z_{\tau i}}} \right\}^{\mathrm{T}} \tag{5}$$

The shape functions are not given here. They can be found in many books, see for example [28]. Elements with four nodes (B4) were adopted in this work, i.e., a cubic approximation ($p = 3$) along the $y$ axis was assumed. The cross-section discretization for the LE class (i.e., the choice of the type, the number, and the distribution of cross-sectional Lagrange elements) is entirely independent of the beam finite element's choice be used along the axis of the beam. The stiffness and mass matrices can be obtained via the principle of virtual displacements; it reads

$$\delta L_{\mathrm{int}} = \int_V \delta\boldsymbol{\epsilon}^{\mathrm{T}}\boldsymbol{\sigma}\, \mathrm{d}V = -\delta L_{\mathrm{ine}} \tag{6}$$

where $L_{\mathrm{int}}$ stands for the strain energy; $L_{\mathrm{ine}}$ is the work of the inertial loadings; $\delta$ stands for the virtual variation; $V = \Omega \times L$ is the volume of the beam; ***epsilon*** and ***sigma*** are the strain and stress vectors, respectively. Using the constitutive laws (i.e. the linear strain displacement relations) and Eq. (4), the virtual variation of the strain energy can be rewritten. It reads

$$\delta L_{\mathrm{int}} = \delta\mathbf{q}_{\tau i}^{\mathrm{T}}\mathbf{K}^{ij\tau s}\mathbf{q}_{sj} \tag{7}$$

where $\mathbf{K}^{ij\tau s}$ is the stiffness matrix in the form of the fundamental nucleus. The derivation of the stiffness matrix's FE fundamental nucleus is not reported here, but it is given in [23], where more details about CUF can also be found. The fundamental nucleus has to be expanded according to the summation indexes $\tau$, $s$, $i$ and $j$ in order to obtain the elemental stiffness matrix. The virtual variation of the work of the inertial loadings is

$$\delta L_{\mathrm{ine}} = \int_V \rho\delta\mathbf{u}^{\mathrm{T}}\ddot{\mathbf{u}}\, \mathrm{d}V \tag{8}$$

where $\rho$ stands for the density of the material, and $\ddot{\mathbf{u}}$ is the acceleration vector. Eq. (8) is rewritten using Eq. (4)

$$\delta L_{\text{ine}} = \delta \mathbf{q}_{\tau i}^{\mathrm{T}} \int_l N_i N_j \mathrm{d}y \int_\Omega \rho F_\tau F_s \mathrm{d}\Omega \, \ddot{\mathbf{q}}_{sj} = \delta \mathbf{q}_{\tau i}^{\mathrm{T}} \mathbf{M}^{ij\tau s} \ddot{\mathbf{q}}_{sj} \tag{9}$$

where $\mathbf{M}^{ij\tau s}$ is the fundamental nucleus of the mass matrix. Its components are provided below, and they are referred to as $M_{rc}^{ij\tau s}$, where $r$ is the row number ($r = 1, 2, 3$) and $c$ denotes column number ($c = 1, 2, 3$).

$$\begin{aligned} \mathbf{M}_{11}^{ij\tau s} &= \mathbf{M}_{22}^{ij\tau s} = \mathbf{M}_{33}^{ij\tau s} = \rho \int_l N_i N_j \mathrm{d}y \int_\Omega F_\tau F_s \mathrm{d}\Omega \\ \mathbf{M}_{12}^{ij\tau s} &= \mathbf{M}_{13}^{ij\tau s} = \mathbf{M}_{21}^{ij\tau s} = \mathbf{M}_{23}^{ij\tau s} = \mathbf{M}_{31}^{ij\tau s} = \mathbf{M}_{32}^{ij\tau s} = 0 \end{aligned} \tag{10}$$

It should be underlined that no assumptions about the approximation order have been made in formulating $\mathbf{K}^{ij\tau s}$ and $\mathbf{M}^{ij\tau s}$. Thus, it is possible to obtain refined beam models without changing the formal expression of the nuclei components. This nuclei's property is the key-point of CUF that allows, with only nine coding statements, to implement any-order of multiple class theories. The undamped dynamic problem is obtained by substituting the fundamental nuclei into the principle of virtual displacement (Eq. (6)), by expanding the CUF fundamental indexes and by assembling the global FEM arrays.

$$\mathbf{M}\ddot{\mathbf{u}} + \mathbf{K}\mathbf{u} = 0 \tag{11}$$

Considering harmonic solutions, the second-order system of ordinary differential equations above results into a classical eigenvalue problem:

$$(-\omega_k^2 \mathbf{M} + \mathbf{K})\mathbf{u}_k = 0 \tag{12}$$

where $\mathbf{u}_k$ is the *kth* eigenvector.

## 3. Component-wise damage modelling

The CUF formulation, in combination with Lagrange polynomials, was recently employed to develop the CW approach [26]. It allows to separately model each component of the structure through 1-D CUF LE formulation. One of CW technique's main advantages is its capability to adjust the model by choosing a more or less detailed model for each component involved, and setting the order for the structural model to be employed. In fact, by enriching the beam kinematics of the structure, higher-order phenomena can be automatically caught. When dealing with models for damage detection, these features could be essential, in order to describe local phenomena as best as possible. In this work, the characteristic of the CW approach of modelling each component of the structure has been exploited for damage detection purposes. In fact, damages with different intensities can be introduced for each part. A basic isotropic damage modelling approach has been used. The damage is introduced through the degradation of the stiffness of the component involved, but it does not affect its mass. Consequently, the material characteristics are modified according to the following:

$$E_d = d \times E, \text{ with } 0 \leq d \leq 1 \tag{13}$$

where E is the Young modulus. In other words:

$$E_1 = E \qquad E_{0.6} = 0.6 \times E \tag{14}$$

An example of damaged structures is illustrated in Fig. 1.

In this work, the method of free vibration analysis has been adopted for structural damage detection. This method is based on the principle that any structural damage causes a change in dynamic parameters, such as natural frequencies, mode shapes and damping. The main challenge is finding how these dynamic parameters are correlated to the damage, in order to build an algorithm capable of predicting damage location and its intensity.

In a recent study [8], the authors demonstrate how it is not possible, for instance, to find a clear correlation between a change in natural frequencies and the presence of damage. In fact, some damage can affect the natural frequencies and not the related mode shapes, or vice versa. Thus, they introduced, alongside the evaluation of the natural frequencies, the use of the Modal Assurance Criterion (MAC) to quantify a mode-to-mode correlation between damaged and undamaged structures. It is calculated as the normalized scalar product of two modal vectors. The resulted scalars are arranged in the MAC matrix:

$$MAC_{ij} = \frac{|\{\phi_{A_i}\}^T \{\phi_{B_j}\}|^2}{\{\phi_{A_i}\}^T \{\phi_{A_i}\} \{\phi_{B_j}\} \{\phi_{B_j}\}^T}$$

where $\{\phi_A\}$ and $\{\phi_B\}$ are the damaged and undamaged modal vector for the $i$th and $j$th modes, respectively. This indicator can take values from 0 (no consistent correspondence) to 1 (consistent correspondence).

In [8], the final objective was to evaluate the effect of damage location and intensity on the structure's vibration characteristic. Here, the inverse problem is posed: the aim is to build a model that, given the free vibration characteristics (Natural frequencies plus MAC matrix), is able to detect location and intensity of all damages in separate components of the structure. This model consists of an ANN, trained through a database of damage scenarios generated by adopting the CW approach.

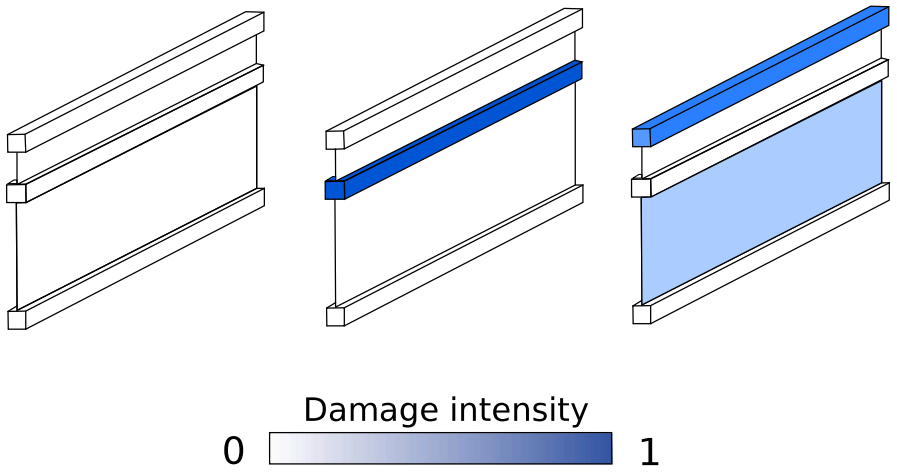


**Fig. 1.** Example of damage introduction in the structure : Undamaged structure (left); one damaged component (centre); two damaged components with different intensities (right).

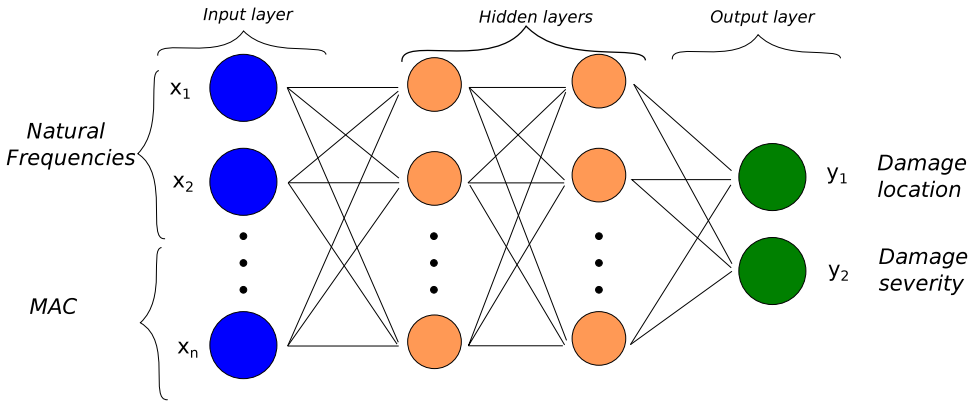


**Fig. 2.** Representation of the architecture of an Artificial Neural Network.

## 4. ANN training for damage detection

An Artificial Neural Network is a group of interconnected neurons. The classical structure of an ANN consists of an input layer, one or more hidden layers, and an output layer. Each layer could have a different number of neurons. Each neuron is connected to all the neurons of the following layer. An example of ANN architecture used in this work is shown in Fig. 2. It is a feedforward neural network, where the transfer functions are the hyperbolic tangent sigmoid for the hidden layer(s) and linear functions for the output layer. An ANN has the ability to learn during the so-called "training process", which aims at reducing the error of the network. The algorithm employed for the ANN training is the Bayesian regularization backpropagation process. In a backpropagation algorithm, once obtained the predicted output, the error between the latter and the desired output is computed. Then, a backward step is performed, and the network parameters are adjusted in order to minimize the error. In the specific case of the Bayesian regularization, the backward step aims at obtaining a trained network with good generalization qualities. Further information about ANN architecture and training process could be found in [29], which has been used as reference for this work.

The determination of damage's presence, the quantification and location of the damage through free vibration analysis require an extensive training database for the neural network, which includes information about the structure's dynamic parameters. Therefore, a considerable number of analysis should be performed. The CW formulation's adoption is essential for providing very accurate analysis with a reduced computational cost, alongside the advantage of having a component-oriented localization of the damage.

In this work, the database has been created through CUF-based Monte Carlo simulations. Damage intensity was assigned randomly to each component, following a Gaussian distribution, with mean equal to 0 and standard deviation equal to 0.1. Therefore, a database of N structures, covering a significant number of possible damage scenarios, has been built. An example of database for a structure with four components is shown in Table 1.

Then, a free vibration analysis has been carried out for all samples. The ANN has used the first natural frequencies and each structure's MAC scalars for its training process. The neural network, when trained, can be used for analysing new structures with a

**Table 1**
Example of database of N samples for a 4-Component structure. The damage introduced for each component is indicated in terms of stiffness reduction (1-d).

| | Component 1 | Component 2 | Component 3 | Component 4 |
|---|---|---|---|---|
| *Sample* 1 | 0.12 | 0.00 | 0.15 | 0.21 |
| *Sample* 2 | 0.20 | 0.07 | 0.01 | 0.15 |
| *Sample* 3 | 0.03 | 0.05 | 0.17 | 0.14 |
| *Sample* 4 | 0.22 | 0.12 | 0.02 | 0.00 |
| *Sample* 5 | 0.16 | 0.15 | 0.01 | 0.09 |
| ... | | ... | ... | |
| ... | | ... | ... | |
| *Sample N* | 0.14 | 0.04 | 0.18 | 0.12 |

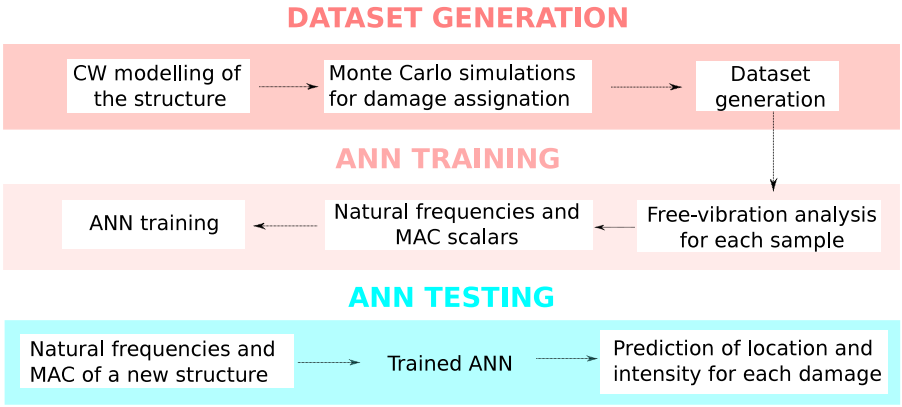


**Fig. 3.** Schematic representing the entire process for damage detection, from the modelling of the structure to the trained ANN.

different damage distribution. Thus, giving as input the first natural frequencies and MAC scalars of this structure, the ANN could predict all damages' location and intensity.

The accuracy of this prediction is strictly related to the ANN architecture. Some studies try to develop optimization method for the design of an ANN architecture [30,31]. Nevertheless, there is not a precise and proved method to define a priori all the parameters. Thus, in this work the network's architecture was built mostly through a trial-error procedure, depending on the problem investigated. The parameters involved were the number of hidden layers and the number of neurons per layer.

Fig. 3 shows a flow chart describing the entire process applied in this work in order to build a network capable of predicting the location and the intensity of a damage in a structure.

## 5. Numerical results

### 5.1. Three-stringer spar

The first case study is a simple longeron with three stiffeners. Its geometry is shown in Fig. 4. The geometrical characteristics of this structure are the following: length L = 3 m, height of the cross section h = 1 m, area of the stringers $A_s = 1.6 \times 10^{-3}$ m, thickness of the panels t = 2 mm and distance between top stringer and middle stringer b = 0.3 m. The longeron is made of an homogeneous and isotropic material, with a Young Modulus E = 75 GPa, a Poisson ratio $\nu = 0.33$ and a density of 2700 kg/m$^3$. The spar is clamped at y = 0 mm.

This case test has already been validated in a previous study [8], for what concerns the computation of the structure's natural frequencies through the CW beam model. In Fig. 5, some representative mode shapes of an undamaged three-stringer spar are illustrated. In Table 2, the values of the 15 frequencies for the undamaged structure and three other damage scenarios are shown. In Fig. 6 the MAC matrices for the mode-to-mode comparison between undamaged and the same three damaged structures are displayed. The last two parameters are fundamental for the training of the ANN.

The FE model used along the longitudinal axis consists of ten B4 elements. The CW model is composed of five L9 elements on the beam cross section, one for each component. They are represented in Fig. 7. In the same figure, the probability density function of the damage intensity for each component is also shown.

Concerning the ANN architecture used for solving this damage detection problem, a sensitivity study has been carried out on two parameters: number of hidden layers (Nl) and number of neurons for each layer (Nn). A training database of 2000 samples has been considered. The results of this study are shown in Fig. 8.

Each bar on the graph represents a simulation with a different neural network, trained through the MATLAB toolbox [32]. In the horizontal axis, the number of the variable parameter is indicated, while the other is kept fixed. On the other hand, the vertical

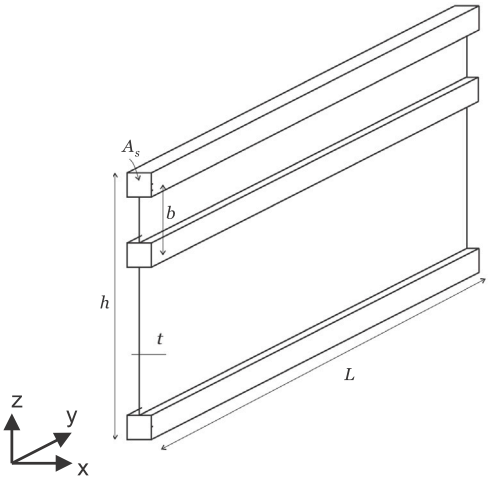


**Fig. 4.** Geometry of three-stringer spar.

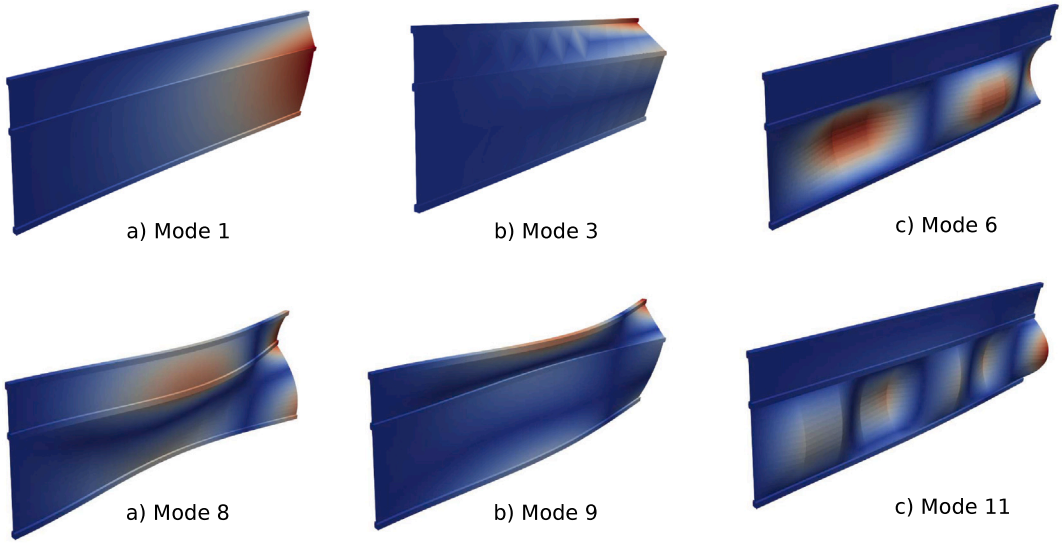


**Fig. 5.** Mode shapes of undamaged Three-stringer spar.

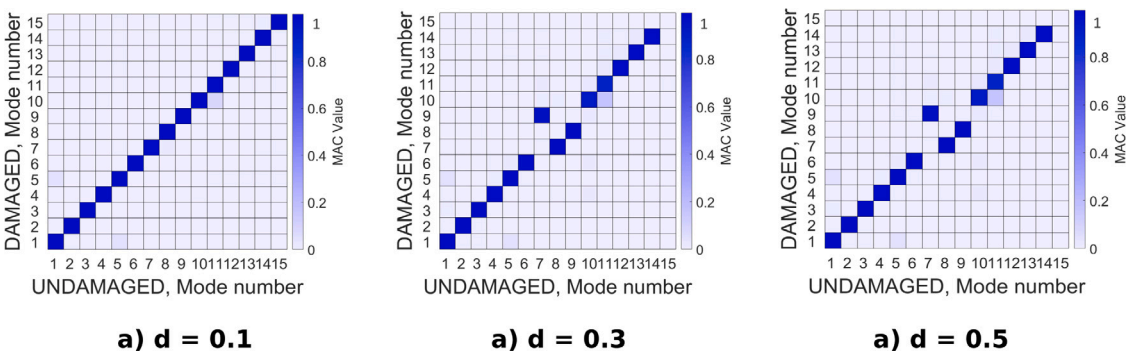


**Fig. 6.** MAC mode-to-mode comparison between undamaged and damaged three-stringer spar for various damage cases.

**Table 2**
First 15 natural frequencies (Hz) of the Three-stinger spar for the undamaged case and three damage scenarios.

| | Undamaged | d = 0.1 | d = 0.3 | d = 0.5 |
|---|---|---|---|---|
| $f_1$ | 3.17 | 3.00 | 2.65 | 2.25 |
| $f_2$ | 3.56 | 3.38 | 3.00 | 2.55 |
| $f_3$ | 3.83 | 3.65 | 3.27 | 2.84 |
| $f_4$ | 14.27 | 13.59 | 12.12 | 10.42 |
| $f_5$ | 16.73 | 15.90 | 14.10 | 12.01 |
| $f_6$ | 17.67 | 16.94 | 15.37 | 13.61 |
| $f_7$ | 21.17 | 20.40 | 18.19 | 15.41 |
| $f_8$ | 21.70 | 20.59 | 18.78 | 16.37 |
| $f_9$ | 22.95 | 21.79 | 19.27 | 16.96 |
| $f_{10}$ | 25.10 | 23.89 | 21.23 | 18.19 |
| $f_{11}$ | 25.75 | 24.85 | 22.98 | 20.94 |
| $f_{12}$ | 31.21 | 30.15 | 27.92 | 25.47 |
| $f_{13}$ | 37.92 | 36.60 | 33.81 | 30.75 |
| $f_{14}$ | 45.79 | 44.13 | 40.61 | 36.73 |
| $f_{15}$ | 54.85 | 52.77 | 48.35 | 41.20 |

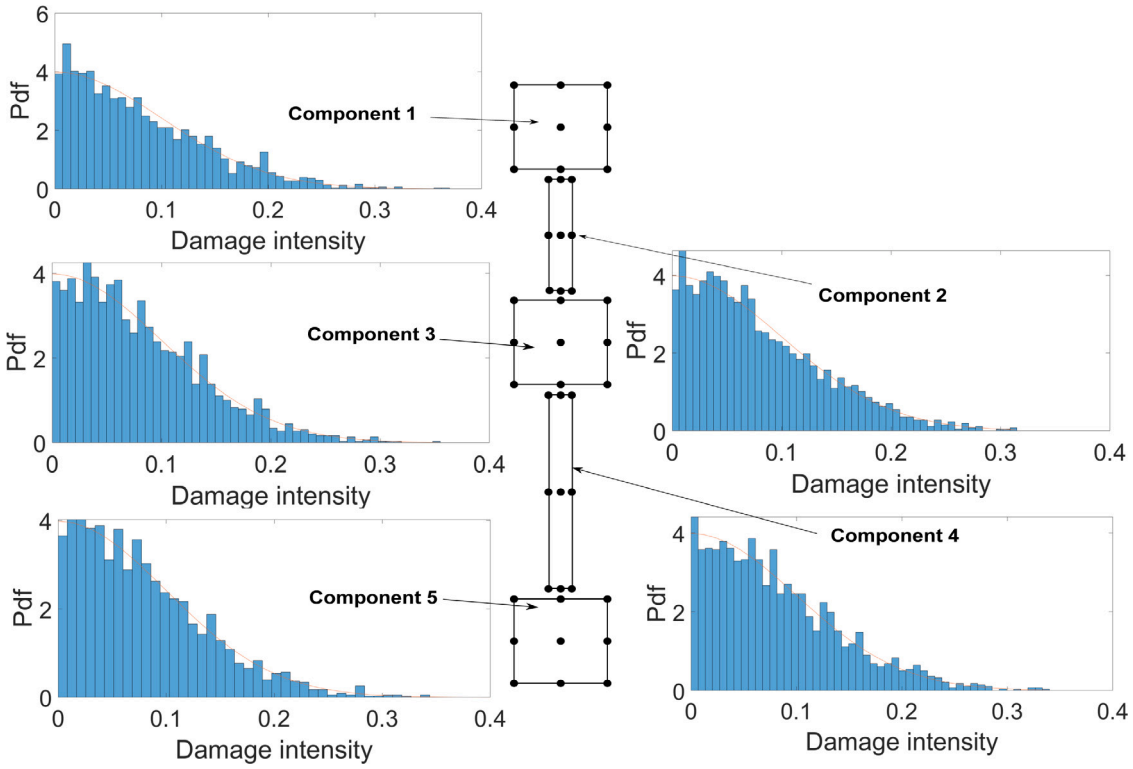


**Fig. 7.** CW model of the Three-Stringer spar and representation of the Gaussian distribution of the damage intensity for each component.

axis shows the Mean Squared Error (MSE) found when the trained net is fed with dynamic parameters of an unseen structure. It reads:

$$MSE = \frac{\sum_{i=1}^{n}(y_i - \hat{y}_i)^2}{n}$$

where $y_i$ represent the target and $\hat{y}_i$ the output of the network. It is a performance index that indicates the accuracy of the neural network in predicting the correct output. The least the value of this index is, the better the neural network is able to guess the desired output. It is important to underline that the computational cost for the neural network training increases when the number of neurons and layers increases. From Fig. 8, it is clear that the best possible result combined with the lowest computational cost is reached when the ANN has two hidden layers with five neurons for each layer. It must be highlighted that only networks whose layers had the same number of neurons have been considered.

Then, the results shown hereafter have been found with a dataset of 2000 samples and a neural network formed by two hidden layers with five neurons.

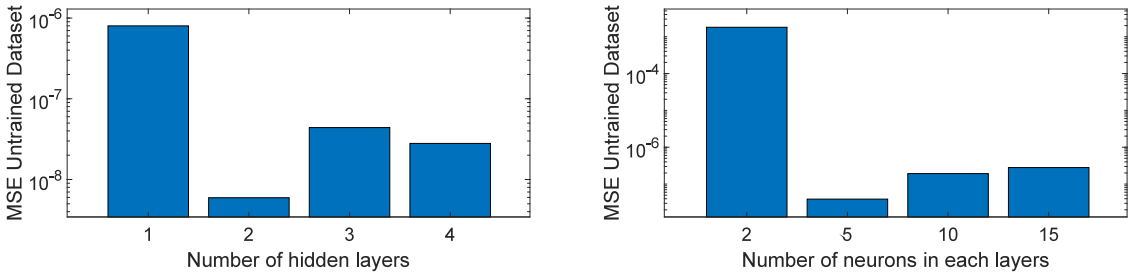


**Fig. 8.** (a) Influence of number of layers (Nn = 5); (b) Influence of number of neurons per layer (Nl = 1).

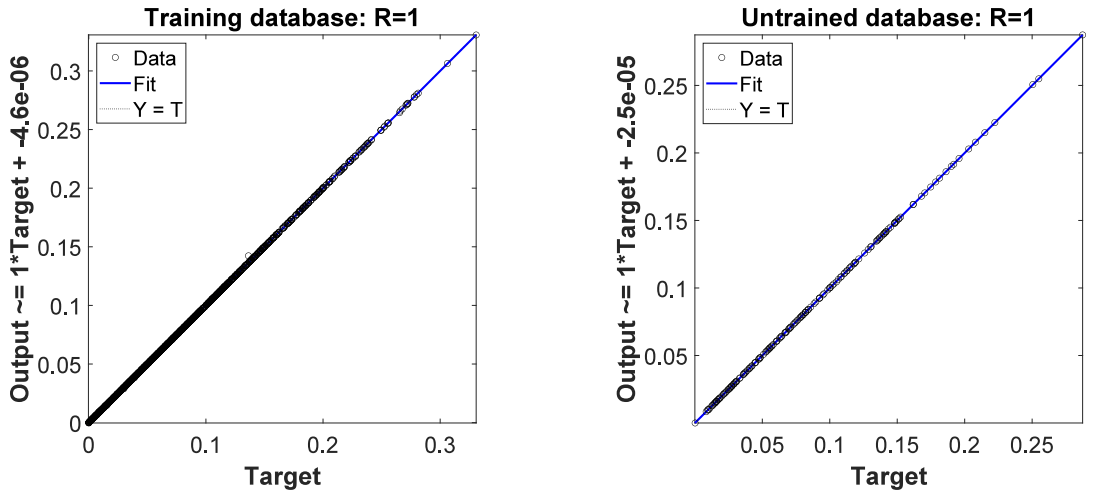


**Fig. 9.** Performance of the ANN with two hidden layers and five neurons in each layer for a three-stringer spar geometry.

The performance of the network is shown in Fig. 9. The coefficient R is the "correlation coefficient". It shows how the predicted output and the targets are linked. It can assume values from 0 to 1, where 1 indicates that the predicted output matches the targets. It can be noticed that this ANN reaches a very high accuracy in predicting damage location and intensity in a three-stringer spar.

Figs. 10–12 show the comparison between the ANN's guess (Blue Bars) and the solution introduced through CUF formulation (Red Bars). In the horizontal axis, the component's numbering is indicated, according to the structure's repartition shown in 7. In the vertical axis the intensity of the damage is displayed.

In Fig. 10, only one component of the structure is damaged, while in Fig. 11 a maximum of two components is damaged at the same time. In Fig. 12 all components are damaged simultaneously. When the damage is introduced in more than one component, its severity can vary from one component to another.

The samples considered in these figures have a damage distribution different from samples used for the training process. Another important consideration to underline about the results shown in Figs. 10 and 11 is the ANN's capability in predicting the component where the damage is present. In other words, when only one or two components are damaged, the ANN is always able to guess the damaged component(s) and the corresponding intensity.

### 5.2. NACA Profile wing

A complete wing is considered as a second assessment. The wing is straight with a NACA 2415 airfoil. The chord $c$ is equal to 1 m. The thickness of each panel is 3 mm, whereas the thickness of the spar webs is 5 mm. The cross-sectional dimensions of the spar caps can be found in [33]. The overall length of the structure is $L = 6$ m. The wing is made of three wing boxes, separated by transversal stiffening members at sections $y = 2$ m, 4 m, and 6 m. The thickness of the ribs is equal to 6 mm. For illustrative purposes, the wing is entirely metallic and the adopted material is an aluminium alloy with the following characteristics: elastic modulus $E = 75$ GPa; Poisson ratio $\nu = 0.33$; and density $\rho = 2700$ kg/m$^3$. The wing is clamped at y = 0 mm. This model was validated in [33].

As for the previous case test, the CW model is adopted. Each longeron, panel, leading and trailing edge are meshed separately, as illustrated in Fig. 13. Nine B4 elements have been used for the discretization along the longitudinal axis, while a combination of L3, L4, and L9 elements has been used for the cross-section. In the same figure, the probability density function of the damage intensity for some components is also shown.

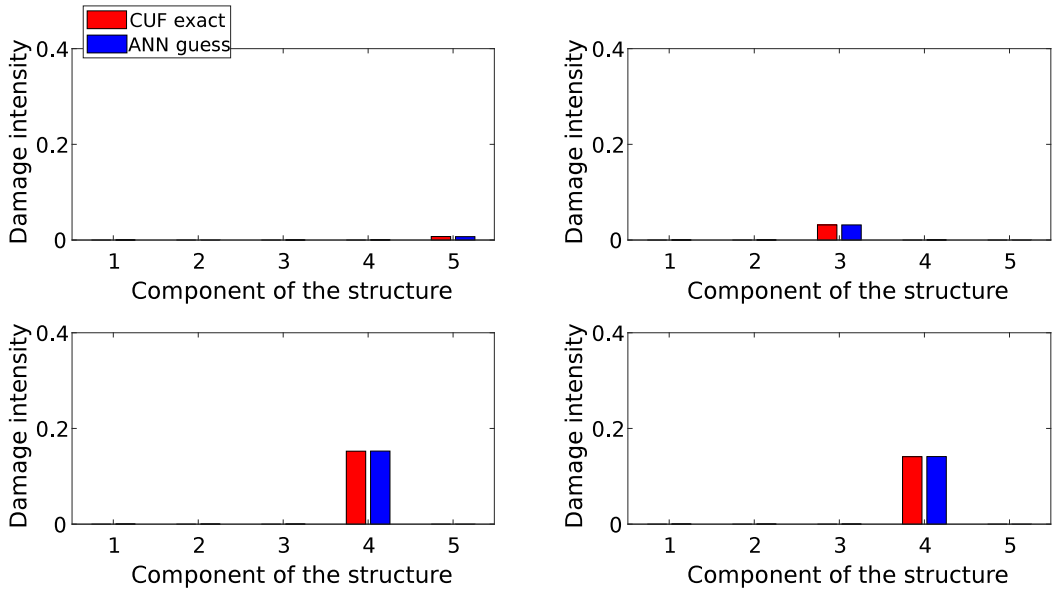


**Fig. 10.** Comparison between the exact CUF solution (Red bars) and the ANN output (Blue bars) for a three-stringer spar. Each graph represents a structure with only one damaged component. (For interpretation of the references to colour in this figure legend, the reader is referred to the web version of this article.)

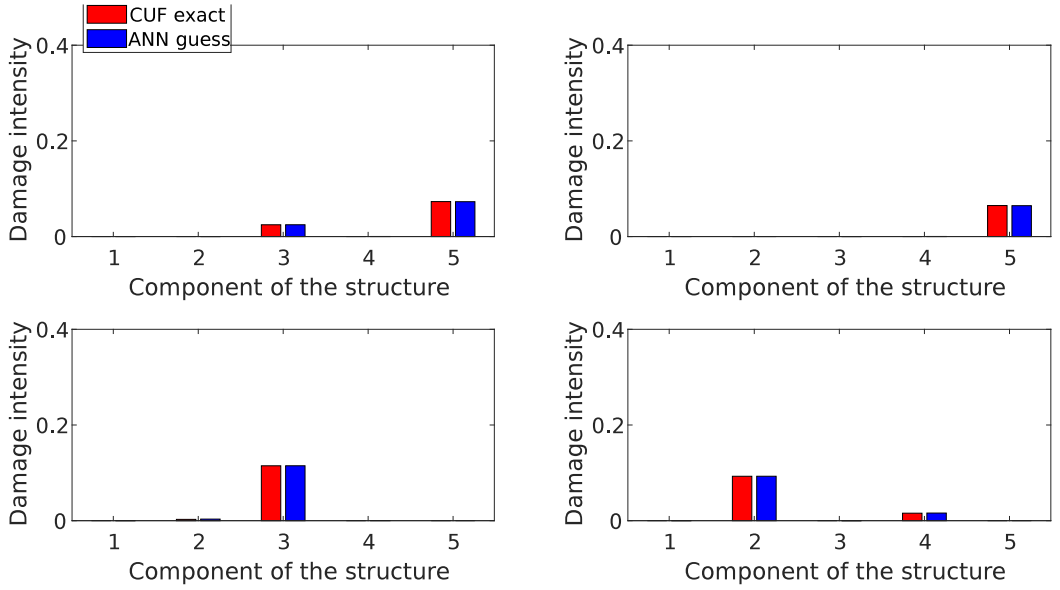


**Fig. 11.** Comparison between the exact CUF solution (Red bars) and the ANN output (Blue bars) for a three-stringer spar. Each graph represents a structure with a maximum of two damaged components. The damage can vary from a component to another. (For interpretation of the references to colour in this figure legend, the reader is referred to the web version of this article.)

In Fig. 14, some representative mode shapes of an undamaged NACA profile wing are illustrated. In Table 3, the values of the 15 frequencies for the undamaged structure and three other damage scenarios are shown. In contrast, in Fig. 15 the MAC matrices for the mode-to-mode comparison between undamaged and the same three damaged structures are displayed.

The adoption of the CW formulation allowed to treat each bay separately. It means that, for instance, the portion of the longeron in the first bay can be damaged while the others stay intact. This modelling leads to having a more precise localization of the damage in the structure. Consequently, there are a total of 18 components that can be damaged, six for each bay. Components of each bay are illustrated in Fig. 16: Leading edge (Component 1), top panel (Component 2), trailing edge (Component 3), rear longeron (Component 4), bottom panel (Component 5) and front longeron (Component 6). No damage was introduced in the three ribs. In fact, the presence of even a small damage in a rib cannot represent an operating condition of this structure.

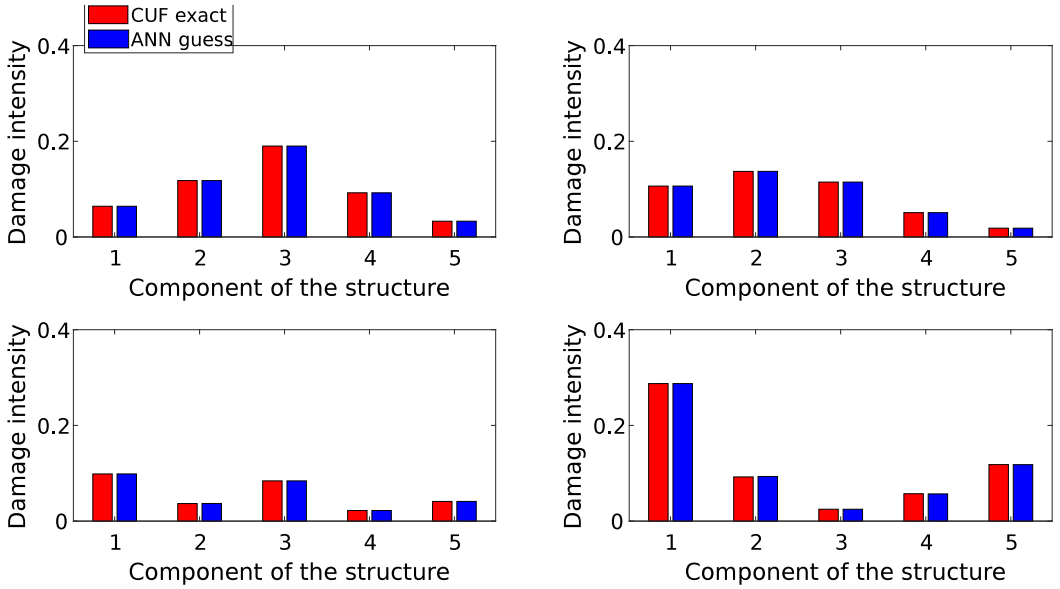


**Fig. 12.** Comparison between exact the CUF solution (Red bars) and the ANN output (Blue bars) for a three-stringer spar. Each graph represents a structure with all components damaged. The damage can vary from a component to another. (For interpretation of the references to colour in this figure legend, the reader is referred to the web version of this article.)

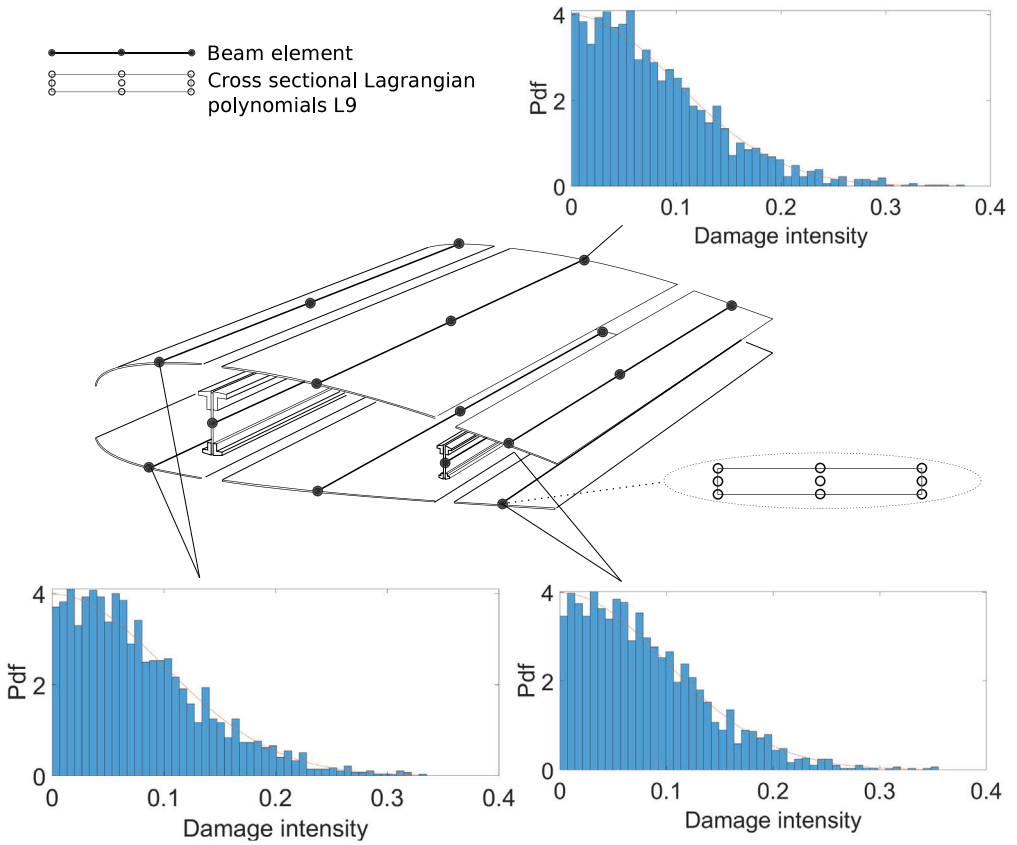


**Fig. 13.** CW model of a NACA profile wing and representation of the Gaussian distribution of the damage intensity for some components.

**Table 3**
First 15 natural frequencies (Hz) of the NACA profile wing for the undamaged case and three damage scenarios.

| | Undamaged | d = 0.1 | d = 0.3 | d = 0.5 |
|---|---|---|---|---|
| $f_1$ | 4.14 | 3.93 | 3.47 | 2.93 |
| $f_2$ | 21.28 | 20.24 | 17.94 | 15.24 |
| $f_3$ | 25.00 | 23.81 | 21.16 | 18.02 |
| $f_4$ | 39.45 | 39.32 | 39.03 | 38.61 |
| $f_5$ | 64.84 | 62.02 | 55.66 | 47.94 |
| $f_6$ | 85.61 | 82.09 | 73.90 | 63.84 |
| $f_7$ | 91.54 | 87.39 | 78.07 | 67.03 |
| $f_8$ | 93.46 | 89.15 | 79.61 | 68.39 |
| $f_9$ | 96.99 | 93.70 | 85.89 | 75.54 |
| $f_{10}$ | 103.67 | 99.45 | 89.85 | 78.23 |
| $f_{11}$ | 104.82 | 100.43 | 90.88 | 79.56 |
| $f_{12}$ | 106.76 | 102.29 | 92.38 | 80.62 |
| $f_{13}$ | 109.90 | 105.69 | 96.42 | 85.06 |
| $f_{14}$ | 115.76 | 111.201 | 100.69 | 87.63 |
| $f_{15}$ | 124.19 | 119.33 | 108.49 | 95.39 |

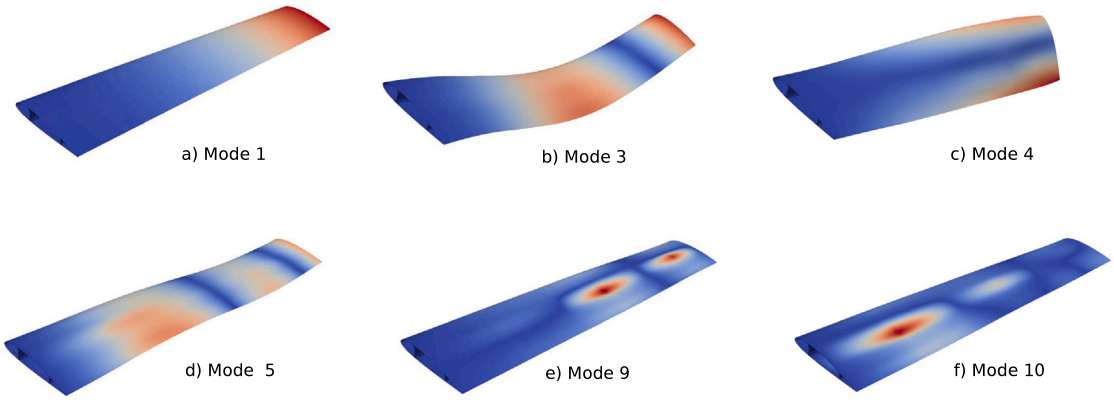


**Fig. 14.** Mode shapes of undamaged NACA profile wing.

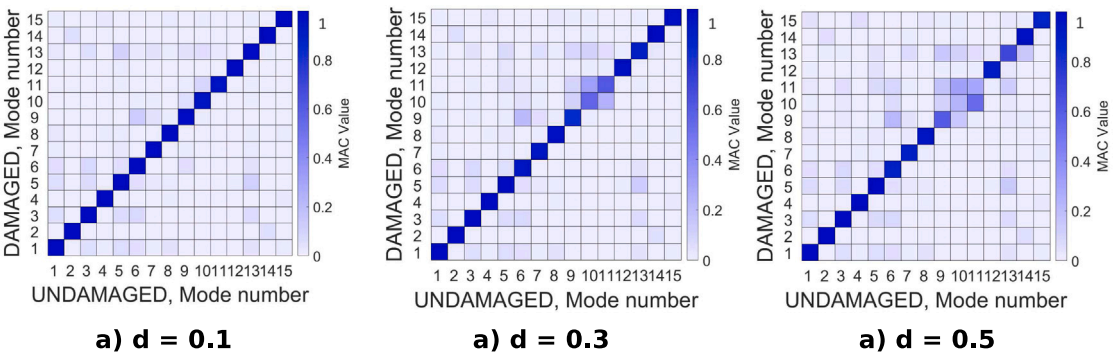


**Fig. 15.** MAC mode-to-mode comparison between undamaged and damaged NACA profile wings for various damage cases.

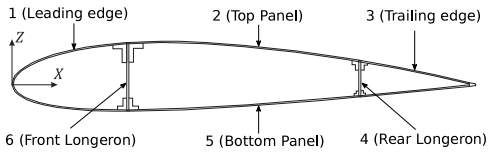


**Fig. 16.** Cross section of the NACA profile wing with the enumeration of the components for a single bay.

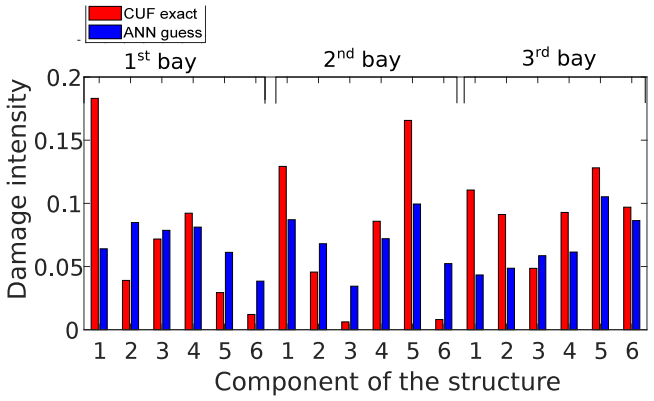


**Fig. 17.** Comparison between the exact CUF solution (Red bars) and the non-optimized ANN (Blue bars) for a profile wing. The ANN architecture used is formed by two hidden layers with five neurons in each one. (For interpretation of the references to colour in this figure legend, the reader is referred to the web version of this article.)

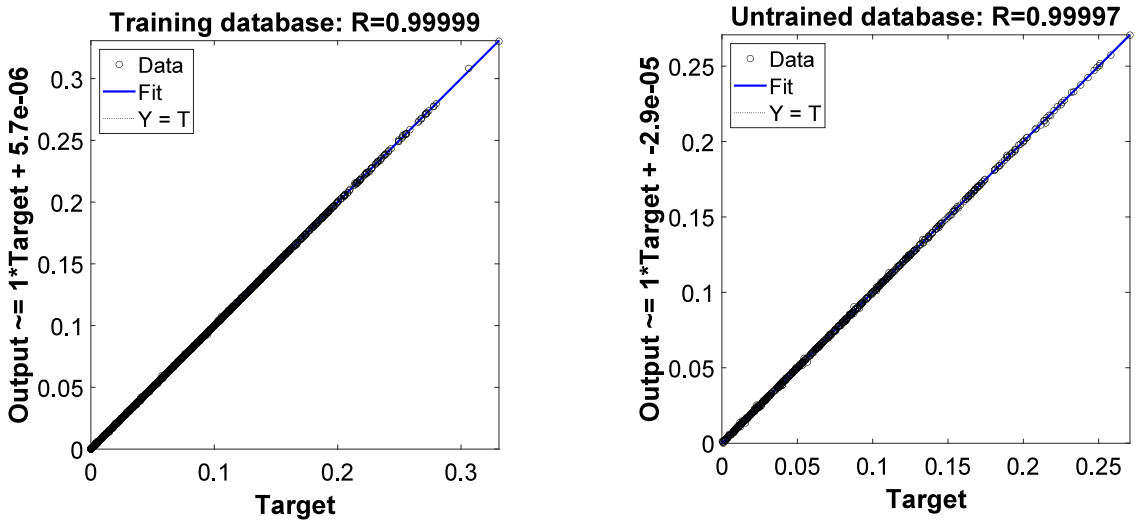


**Fig. 18.** Performance of the ANN with three hidden layers and 28 neurons in each layer for a profile wing.

The dataset used for the training of the ANN consisted of 2000 samples. Each sample was a structure with a different damage distribution.

The first network's architecture tested is the same used in the three-stringer spar case. It was formed by two hidden layers with five neurons for each layer. All 18 components were damaged at the same time. Results are shown in Fig. 17. The component's numbers go from 1 to 6 for each bay, following the numeration introduced in Fig. 16.

It is evident that this network, which was very accurate for the previous case test, is not suitable for this problem. The correlation coefficient R is around 0.5. The reason is that, even if the number of input and output does not change, the FEM model is now more complex and the number of components involved increased from 5 to 18. Thus, a trial-and-error procedure was carried out in order to find the best architecture possible. The resultant ANN was formed by three hidden layers, each one composed of 28 neurons. The input and the output were 15 natural frequencies plus the MAC scalars, as for the previous case test.

In Fig. 18, the performance of this network is shown. The neural network predicts with great accuracy damage location and intensity. A more in-depth analysis shows that the network finds small discrepancies in predicting damage location and severity in components with very small defects.

Figs. 19 and 20 show the comparison between the CUF exact solution (Red bars) and the network's output (Blue bars) when only one or two components were damaged. The damaged components could also be in two different bays. The structures investigated in these figures had a damage distribution that was not used for the ANN training. It means that this input is new for the trained neural network. Therefore, the ANN is able to predict with a very high accuracy damage location and intensity even in a more complex structure like a wing profile.

Fig. 21 shows the results of the ANN when all components are damaged simultaneously. The same hypothesis for Figs. 19 and 20 have been made.

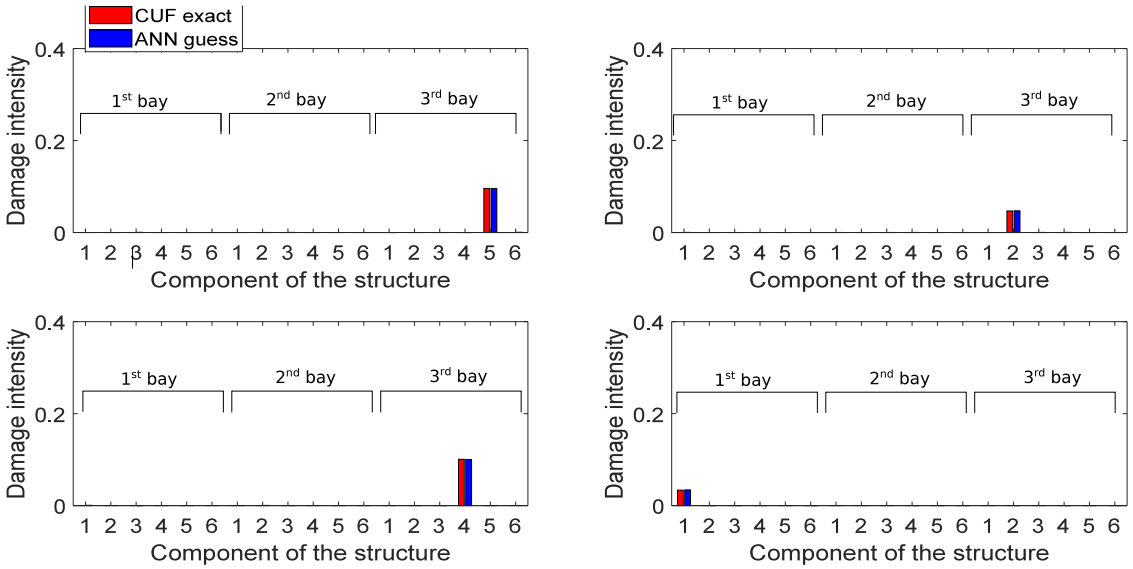


**Fig. 19.** Comparison between the exact CUF solution (Red bars) and the optimized ANN (Blue bars) for a profile wing. Each graph represents a structure with only one damaged component. (For interpretation of the references to colour in this figure legend, the reader is referred to the web version of this article.)

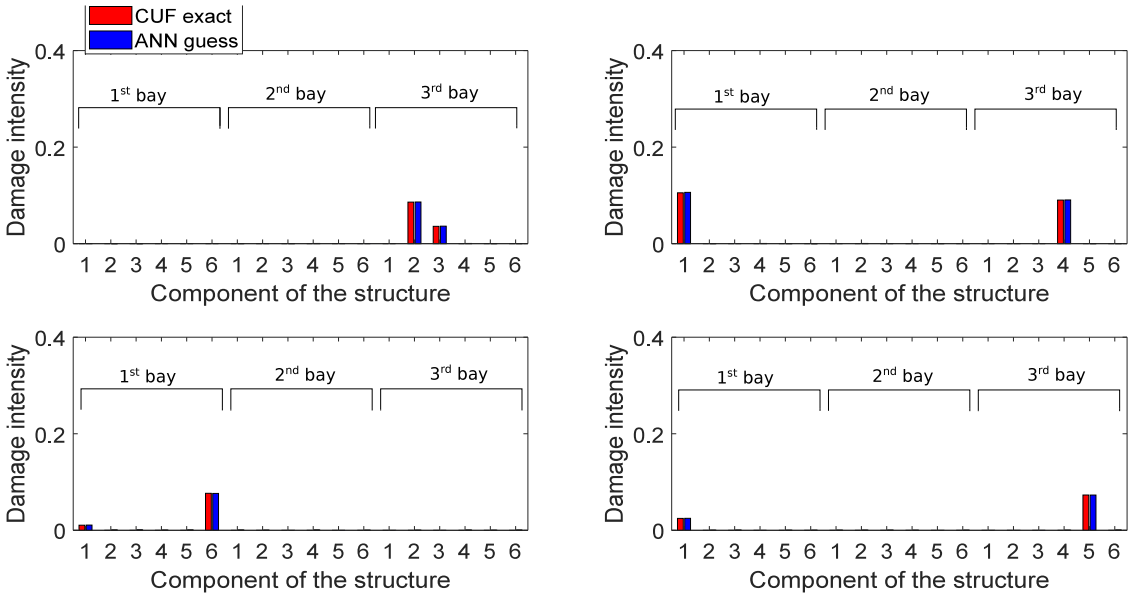


**Fig. 20.** Comparison between the exact CUF solution (Red bars) and the optimized ANN (Blue bars) for a profile wing. Each graph represents a structure with a maximum of two damaged components. The damage can vary from a component to another. (For interpretation of the references to colour in this figure legend, the reader is referred to the web version of this article.)

## 6. Conclusions

This work proposed a damage detection method based on Artificial Neural Networks (ANN) and a one-dimensional free vibration analysis model. The latter is based on the study of Carrera et al. in [8]. In fact, the analyses were carried out through a CW formulation. CW models' adoption allows a better description of higher order and local phenomena, an important characteristic for damage detection.

The damage was introduced in the structure by the degradation of the stiffness of its components. A databases of a certain number of structures with different damage distribution has been built through Monte Carlo simulations. For each sample, a free vibration analysis was performed. The output of these analysis (natural frequencies and MAC matrix) was used for the training of the ANN. The choice of using the MAC as input is made because it gives essential information about the mode shape evolution, which cannot

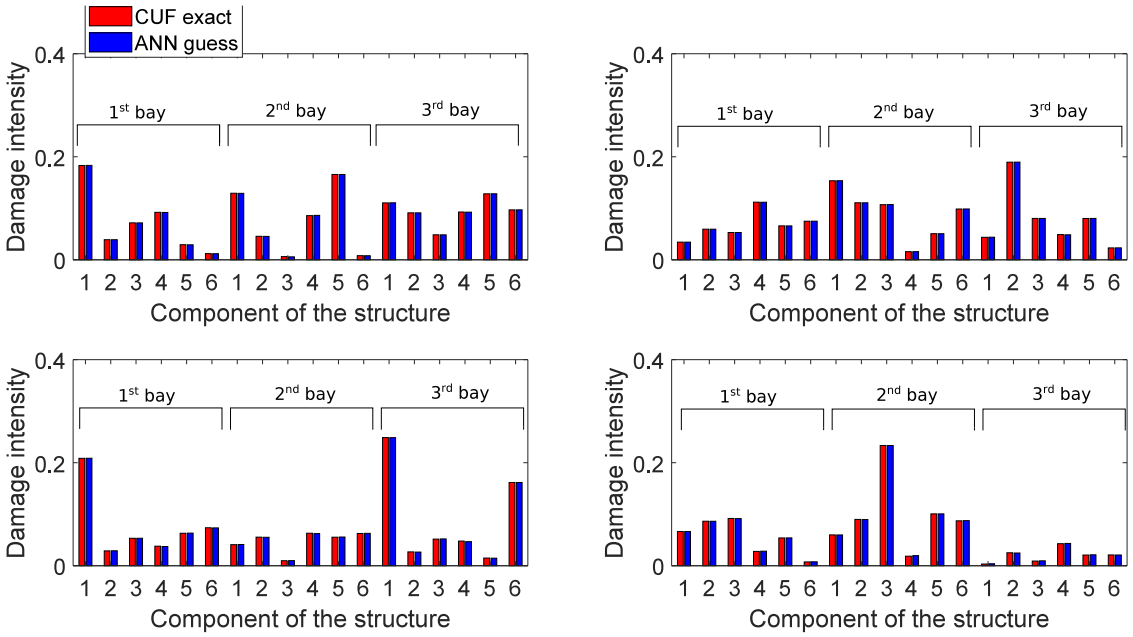


**Fig. 21.** Comparison between the exact CUF solution (Red bars) and the optimized ANN (Blue bars) for a profile wing. Each graph represent a structure with all components damaged. The damage can vary from a component to another. (For interpretation of the references to colour in this figure legend, the reader is referred to the web version of this article.)

be caught via the shift in natural frequencies only. Thus, given a set of these vibration data, trained ANN were employed to detect damage location and intensities in structures whose health status was unknown.

This approach was tested on two different geometries. The results suggest that:

- ANN's can detect with great accuracy damage location and severity in each component of the structure. It should be underlined that ANN training is computationally affordable because high order 1D finite elements are used for generating data, whereas the resolution of the inverse problem is immediate.
- The proposed component-oriented approach can guarantee a better localization of the damage. It is possible to artificially divide a component into other sub-components, making the model more precise. Nevertheless, increasing the number of components leads to a more complex problem and, by consequence, to a more complex ANN. A trade-off point between precision and complexity has to be found.

The CUF and CW models employed showed to be very interesting for damage detection. Nevertheless, note that the effectiveness of the proposed method is subjected to two main hypotheses: (i) the damage only affects the stiffness of the structure, and not the mass; (ii) modal shapes and natural frequencies can be measured on-site in such a precise way to be feed within a simulation-based trained ANN.

In this work, only isotropic damages have been considered. The next step could be implementing a model that takes into account also anisotropic damages in the structure. Another further development could be the training of ANN's capable of detecting damage location and intensity by introducing as input the frequencies of the structure subjected to a load corresponding to its operating conditions. Finally, recent studies (i.e. [34,35]) are moving towards the use of hybrid (experimental and numerically generated, as in [36,37]) data for ANN training process. Thus, another step could be the addition of some experimental data as input for the training process, in order to investigate the effects of measurements errors on the accuracy of ANN predictions.

## CRediT authorship contribution statement

**A. Pagani:** Conceptualization, Methodology, Software, Writing - review & editing, Supervision, Project administration, Funding acquisition. **M. Enea:** Software, Validation, Formal analysis, Investigation, Writing - original draft. **E. Carrera:** Conceptualization, Methodology, Writing - review & editing, Supervision, Project administration, Funding acquisition.

## Declaration of competing interest

The authors declare that they have no known competing financial interests or personal relationships that could have appeared to influence the work reported in this paper.

## Acknowledgements

AP acknowledges funding from the European Research Council (ERC) under the European Union's Horizon 2020 research and innovation programme (Grant agreement No. 850437). ME and EC acknowledge the DEVISU project, supported by the *Ministero dell'Istruzione, dell'Università e della Ricerca* research funding programme PRIN 2017 (2017ZX9X4K).

## References

[1] M. Mitra, S. Gopalakrishnan, Guided wave based structural health monitoring: A review, Smart Mater. Struct. 25 (5) (2016) http://dx.doi.org/10.1088/0964-1726/25/5/053001.
[2] G. Kahandawa Appuhamillage, J. Epaarachchi, H. Wang, K.T. Lau, Use of FBG sensors for SHM in aerospace structures, Photonic Sensors 2 (2012) http://dx.doi.org/10.1007/s13320-012-0065-4.
[3] S.Z. Zhang, Y.J. Yan, Z. Wu, Electric potential detection for structural surface crack using coating sensors, Sensors Actuators A 137 (2007) 223–229, http://dx.doi.org/10.1016/j.sna.2007.03.001.
[4] C. Hirwani, S. Panda, Nonlinear transient analysis of delaminated curved composite structure under blast/pulse load, Eng. Comput. 36 (2020) http://dx.doi.org/10.1007/s00366-019-00757-6.
[5] A. Labib, D. Kennedy, C. Featherston, Free vibration analysis of beams and frames with multiple cracks for damage detection, J. Sound Vib. 333 (20) (2014) 4991–5003.
[6] R. Capozuzza, Vibration of CFRP cantilever beam with damage, Compos. Struct. 116 (2014) 211–222.
[7] Y. Yan, Q. Ren, N. Xia, L. Zhang, A close-form solution applied to the free vibration of the Euler–Bernoulli beam with edge cracks, Arch. Appl. Mech. 86 (2016) http://dx.doi.org/10.1007/s00419-016-1140-x.
[8] E. Carrera, A. Pagani, M. Petrolo, Free vibrations of damaged aircraft structures by component-wise analysis, AIAA J. 54 (2016) 1–16, http://dx.doi.org/10.2514/1.J054640.
[9] A. Viglietti, E. Zappino, E. Carrera, Free vibration analysis of locally damaged aerospace tapered composite structures using Component-Wise models, Compos. Struct. 192 (2018) http://dx.doi.org/10.1016/j.compstruct.2018.02.054.
[10] E. Carrera, A. Pagani, Free vibration analysis of civil engineering structures by Component-Wise models, J. Sound Vib. 333 (2014) 4597–4620, http://dx.doi.org/10.1016/j.jsv.2014.04.063.
[11] J.B. Kosmatka, Ricles J.M., Damage detection in structures by modal vibration characterization, J. Struct. Eng. (ISSN: 0733-9445) 125 (1999) http://dx.doi.org/10.1061/(asce)0733-9445(1999)125:12(1384).
[12] M.M. Fayyadh, H.A. Razak, Z. Ismail, Combined modal parameters-based index for damage identification in a beamlike structure: theoretical development and verification, Arch. Civil Mech. Eng. 11 (3) (2011) 587–609.
[13] N.T. Khiem, T.V. Lien, Multi-crack detection for beam by the natural frequencies, J. Sound Vib. 273 (2004) 175–184, http://dx.doi.org/10.1016/S0022-460X(03)00424-3.
[14] R. Ruotolo, C. Surace, Damage assessment of multiple cracked beams: Numerical results and experimental validation, J. Sound Vib. (ISSN: 0022460X) 206 (1997) http://dx.doi.org/10.1006/jsvi.1997.1109.
[15] M. Şahin, R. Shenoi, Quantification and localisation of damage in beam-like structures by using artificial neural networks with experimental validation, Eng. Struct. 25 (2003) 1785–1802, http://dx.doi.org/10.1016/j.engstruct.2003.08.001.
[16] M. Şahin, R. Shenoi, Vibration-based damage identification in beam-like composite laminates by using artificial neural networks, J. Mech. Eng. Sci. 217 (2003) 661–676, http://dx.doi.org/10.1243/095440603321919581.
[17] H. Das, D. Parhi, Application of neural network for fault diagnosis of cracked cantilever beam, in: 2009 World Congress on Nature and Biologically Inspired Computing, NABIC 2009 - Proceedings, 2010, pp. 1303–1308, http://dx.doi.org/10.1109/NABIC.2009.5393733.
[18] S. Suresh, S.N. Omkar, R. Ganguli, V. Mani, Identification of crack location and depth in a cantilever beam using a modular neural network approach, Smart Mater. Struct. 13 (2004) http://dx.doi.org/10.1088/0964-1726/13/4/029.
[19] K. Sumangala, Damage assessment of prestressed concrete beams using Artificial Neural Network (ANN) approach, Comput. Struct. 84 (2006) 1709–1718, http://dx.doi.org/10.1016/j.compstruc.2006.03.005.
[20] R.A. Saeed, A. Galybin, V. Popov, Crack identification in curvilinear beams by using ANN and ANFIS based on natural frequencies and frequency response functions, Neural Comput. Appl. 21 (2012) 1629–1645, http://dx.doi.org/10.1007/s00521-011-0716-1.
[21] K. Aydin, O. Kisi, Damage diagnosis in beam-like structures by artificial neural networks, J. Civ. Eng. Manage. (ISSN: 18223605) 21 (2015) http://dx.doi.org/10.3846/13923730.2014.890663.
[22] H. Fathnejat, P. Torkzadeh, E. Salajegheh, R. Ghiasi, Structural damage detection by model updating method based on cascade feed-forward neural network as an efficient approximation mechanism, Int. J. Optim. Civ. Eng. 4 (2014) 451–472.
[23] E. Carrera, M. Cinefra, M. Petrolo, E. Zappino, Finite Element Analysis of Structures Through Unified Formulation, John Wiley & Sons, ISBN: 978-1-119-94121-7, 2014.
[24] E. Carrera, G. Giunta, M. Petrolo, Beam Structures: Classical and Advanced Theories, John Wiley & Sons, 2011, http://dx.doi.org/10.1002/9781119978565.
[25] R.J. Allemang, D. Brown, A Correlation Coefficient for Modal Vector Analysis, 1982.
[26] E. Carrera, M. Petrolo, Refined beam elements with only displacement variables and plate/shell capabilities, Meccanica 47 (3) (2012) 537–556, http://dx.doi.org/10.1007/s11012-011-9466-5.
[27] E. Oñate, Structural Analysis with the Finite Element Method: Linear Statics, Vol. 1, Springer, 2009.
[28] K.J. Bathe, Finite Element Procedure, Prentice hall, 1996.
[29] H.B. Demuth, M.H. Beale, O. De Jess, M.T. Hagan, Neural Network Design, second ed., Martin Hagan, ISBN: 0971732116, 2014.
[30] P. Benardos, G. Vosniakos, Optimizing feedforward artificial neural network architecture, Eng. Appl. Artif. Intell. 20 (2007) 365–382, http://dx.doi.org/10.1016/j.engappai.2006.06.005.
[31] J. Arifovic, R. Gençay, Using genetic algorithms to select architecture of a feedforward artificial neural network, Physica A 289 (2001) 574–594, http://dx.doi.org/10.1016/S0378-4371(00)00479-9.
[32] Inc. The MathWorks. Deep learning toolbox. Natick, Massachusetts, United State, 2020. URL https://www.mathworks.com/help/symbolic/.
[33] E. Carrera, A. Pagani, M. Petrolo, Component-wise method applied to vibration of wing structures, J. Appl. Mech. 80 (4) (2013) 041012, http://dx.doi.org/10.1115/1.4007849.
[34] T. Yamashita, M. Kohiyama, K. Watanabe, Deep neural network for detecting earthquake damage to brace members installed in a steel frame, Japan Archit. Rev. 4 (1) (2021) 56–64.
[35] H. Khodabandehlou, G. Pekcan, S. Fadali, Vibration-based structural condition assessment using convolution neural networks, Struct. Control Health Monit. 26 (2018).
[36] H. Dewangan, N. Sharma, C. Hirwani, S. Panda, Numerical eigenfrequency and experimental verification of variable cutout (square/rectangular) borne layered glass/epoxy flat/curved panel structure, Mech. Based Des. Struct. Mach. (2020) 1–18, http://dx.doi.org/10.1080/15397734.2020.1759432.
[37] M. Kunche, P. Mishra, H. Nallala, C. Hirwani, P. Katariya, Subhransu Panda, Subrata Panda, Theoretical and experimental modal responses of adhesive bonded T-joints, Wind Struct. 29 (2019) 361–369, http://dx.doi.org/10.12989/was.2019.29.5.361.